



Assessing thermodynamic models and introducing novel method for prediction of methane hydrate formation

Mohamad Mohamadi-Baghmolaei¹ · Abdollah Hajizadeh¹ · Reza Azin² · Amir Abbas Izadpanah¹

Received: 10 August 2017 / Accepted: 26 November 2017 / Published online: 12 December 2017
© The Author(s) 2017. This article is an open access publication

Abstract

Transmission of natural gas with methane as the main constituent has been a subject of interest to industrial companies. Predicting hydrate formation conditions is important to prevent formation of methane hydrate in gas pipeline. Also, attention has been taken to account for capture and storage of pure methane. In this paper, a comprehensive comparison is performed between empirical correlations and different equation of state in van der Waals Platteeuw (VdW-P) thermodynamic model to determine the most accurate method of hydrate formation condition of methane. In addition, a novel, simple and accurate correlation is developed to predict methane hydrate formation temperature using genetic programming. Error analysis on a wide range of experimental data indicates that the new proposed correlation is superior over existing correlations and all VdW-P models with $R^2 = 0.999$.

Keywords Empirical correlation · VdW-P · Hydrate formation · Methane · Genetic programming

List of symbols

A, B	Fitted constants (K/atm, K)
a	Activity
C	Langmuir constant (1/atm)
C_p	Specific heat capacity, (cal/mol K)
f	Fugacity (bar)
M	Types of cavity
N	The number of types of cavities in crystalline hydrate lattice
NH	The number of gas type molecules which can entry the hydrate phase and fill the cavities
v	The number of cavities of type i per water molecule in the lattice
V	Molar volume (cm^3/mol)
μ	Chemical potential (J/mol)
\emptyset	Fugacity coefficient

Abbreviations

HFP	Hydrate formation pressure
HFT	Hydrate formation temperature
AARE	Average absolute error
R^2	Squared correlation coefficient
RMSE	Root-mean-squared error
RSS	Residual sum of square

Subscripts

w	Water
g	Gas
j, i	Components j, i
jm	Component m in cavity j

Superscripts

V	Vapor phase
L	Liquid phase
H	Hydrate phase
β	Virtual phase
$\beta - L$	Difference between crystalline hydrate lattice and liquid
$\beta - H$	Difference between crystalline hydrate lattice and hydrate

✉ Reza Azin
reza.azin@pgu.ac.ir

¹ Department of Chemical Engineering, Faculty of Petroleum, Gas and Petrochemical Engineering, Persian Gulf University, Bushehr, Iran

² Department of Petroleum Engineering, Faculty of Petroleum, Gas and Petrochemical Engineering, Persian Gulf University, Bushehr, Iran

Introduction

The gas hydrates are pseudo-ice structured compounds which consist of water molecules and natural gas components. The natural gas components act as guest trapped in cage-like structure formed by water (Sloan and Koh 2007; Bahadori and Vuthaluru 2009). Generally, hydrate is generated at specific low temperature and high pressure which are affected by gas composition. Hydrate formation usually causes unfavorable effects such as obstruction in pipelines, gas tubing wells and in surface facilities (Elgibaly and Elkamel 1998). C_2^+ recovery from natural gas is an economic process through which methane with high purity is separated from other hydrocarbons, and is subject to hydrate formation in presence of water. Hence, any effort which facilitates prevention of unsolicited phenomenon such as methane hydrate formation in gas transmission pipeline should be taken into consideration (Koh et al. 2002). High energy demand persuades countries like China, Japan, India and South Korea to explore and exploit methane hydrate resources (Collett 2002; Vedachalam et al. 2015; Konno et al. 2016). It was understood that methane hydrate-bearing sandy sediments are found in the Japan, South Korea, India and USA (Ruppel et al. 2008; Ryu et al. 2013; Collett et al. 2014; Fujii et al. 2015). Several researchers tried to explore different aspects of methane hydrate formation conditions. Zhong et al. investigated separating methane from a coal mine methane gas using gas hydrate crystallization method (2016). This was due to large gas storage capacity of methane hydrate and finding average formation conditions. Their proposed method was promising for separation of gas mixtures. Another illustration is that of Zhong et al. (2015) who used gas hydrate formation for CO_2 removal from a simulated shale gas. Moreover, methane hydrate formation as a huge source of energy was the aim of study indifferent researches especially to evaluate enhancement of methane hydrate growth and its density. As an example, Ganji et al. used a surfactant to decrease surface tension of water. Results of their study showed that methane hydrate formation rate and storage capacity increased effectively (Ganji et al. 2007). Several studies focus on the rate of methane hydrate formation in presence of different chemicals and porous materials (Liang et al. 2005, 2009a, b; Yan et al. 2005; Ganji et al. 2007; Park and Kim 2010; Babu et al. 2013; Chari et al. 2013; Pasieka et al. 2013; Lim et al. 2014, Siangsai et al. 2014, 2015).

Studies of hydrate formation prediction are presented in two general categories, thermodynamic models and empirical correlations. In addition, use of intelligent models is extended recently for prediction of physical properties of energy sources (Mohamadi-Baghmolaei et al. 2014, 2015).

Mathematical-based equations and thermodynamic relations are proposed for use in simulation process and program code where the relationship between input and output is pretty clear. Common thermodynamic models for hydrate formation are K value method and van der Waals Platteeuw (Wilcox et al. 1941; Van der Waals and Platteeuw 2007). The first method is developed based on vapor–solid equilibrium constants for prediction of hydrate formation condition, while the second is based on statistical thermodynamic approach. The main drawback of thermodynamic models is their weak ability in prediction of high and low pressure and temperature. Also, thermodynamic models are complicated to be programmed and applied (Garapati and Anderson 2014). Application of thermodynamic models as function of equation of state including several components is considerably time taking process as the inter-molecular interaction and proper mixing rules should be estimated through trial and error process (Mohamadi-Baghmolaei et al. 2014, 2016a). In the case of empirical correlations, the input parameters include temperature, pressure and gas gravity. These methods are useful for rapid estimation of the hydrate formation conditions. Moreover, less input data make them easy to use for industrial and practical purposes (Carroll 2014). For instance, Hammerschmidt presented a simple empirical correlation for hydrate formation which was independent of gas gravity (1934). This correlation shown in Eq. (1) is function of pressure (psi) and results the temperature ($^{\circ}F$) of hydrate formation. The simplicity of Hammerschmidt (HSCH) correlation may cause deviation from experimental data.

$$T = 8.9P^{0.285} \quad (1)$$

Another example is Holder et al.'s (1988) correlation developed for predicting hydrate formation pressure which was simple and easy to use. Their correlation depends on two coefficients which are function of temperature range for each gas. These coefficients can be determined by curve fitting on experimental data.

$$P = \exp\left(38.9803 + \frac{-8533.80}{T}\right) \quad (2)$$

Some empirical correlations contain large number of coefficients in their equations. For example, Kobayashi et al. (1987) proposed their correlation with fifteen coefficients. Other example in the same category is the presented correlation by Amin et al. (2015) which was developed based on leverage approach or Ghiasi (2012) who offered a correlation as a function of molecular weight and pressure to predict hydrate formation temperature (HFT). Ghiasi developed his correlation for prediction of hydrate formation temperature (HFT) (K) of sweet natural gases. The correlation depends on pressure (kPa) and molecular weight (M_w).

$$T = A_0 + A_1M_w + A_1M_w^2 + A_4(\ln P)^2 + A_5M_w \ln P \tag{3}$$

The coefficients of Eq. (3) are reported by Ghiasi (2012).

There are other correlations published in the literature which are tested in this paper. Details of these correlations are given in “Empirical correlations” appendix section.

In the current study, a comprehensive comparison is performed between empirical correlations and van der Waals Platteeuw (VdW-P) model. Application of VdW-P EOS is described for fugacity calculation. To do this, seven equations of state (EOS) including Virial, van der Waals (VdW), Redlich–Kwong (RK), Soave–Redlich–Kwong (SRK), Peng–Robinson (PR), Tsai–Jan (TJ) and Patel–Teja (PT) (Van der Waals 1873; Redlich and Kwong 1949; Soave 1972; Peng and Robinson 1976; Patel and Teja 1982; Tsai and Jan 1990; Prausnitz et al. 1998) are employed in VdW-P model to find an accurate method for predicting hydrate formation pressure (HFP) and HFT in temperature range of 259.1–320.1 (K). The accuracy of each model is validated using pure methane hydrate formation experimental data of temperature and pressure. Finally, new empirical correlation is developed for HFT of pure methane.

Van der Waals Platteeuw model

The VdW-P thermodynamic model which was proposed for hydrate formation conditions. This model is based on the following assumptions (Chen and Guo 1996):

1. Each cavity should contain at most one guest (gas) molecule.
2. The ideal gas partition function is applicable to guest molecules.
3. The interaction between guest and water molecules can be described by a pair potential function, and the cavity can be treated as perfectly spherical.
4. Guest–guest molecule interactions are neglected.
5. There is no interaction between guest molecules in different cavities, and the guest molecules interact only with the nearest neighboring water molecules.
6. The free energy contribution of water molecules is independent of the modes of occupancy of dissolved guest molecules.

Thermodynamic equilibrium suggests that chemical potentials of each component in liquid, solid (hydrate) and vapor (L_w-H-V) should be equal. This results in equality of fugacities which is the condition of equilibrium state. The fugacity and chemical potential of each term are denoted by f (bar) and μ (J/mol), respectively.

$$\mu_g^L(P, T) = \mu_g^V(P, T) = \mu_g^H(P, T) \tag{4}$$

$$\mu_w^L(P, T) = \mu_w^V(P, T) = \mu_w^H(P, T) \tag{5}$$

The chemical potential difference between hydrate and virtual phase (β) is:

$$\mu_w^{\beta-H}(P, T) = \mu_w^\beta(P, T) - \mu_w^H(P, T) \tag{6}$$

The potential difference of Eq. 3 is calculated using a statistical relation developed for gas hydrate (Van der Waals and Platteeuw 2007). It was assumed that the solid phase can be modeled by inspiring from the Langmuir gas adsorption model.

$$\mu_w^{\beta-H}(P, T) = RT \sum_{m=1}^N v_m \ln \left(1 + \sum_{j=1}^{NH} C_{jm} f_j^v \right) \tag{7}$$

where R , T , v , C and f are universal gas constant, temperature, number of type- m cavities per water molecule in the lattice, the Langmuir constant and pure fugacity of component j . The number of types of cavities in crystalline hydrate lattice, types of cavity and number of gas type molecules which can enter the hydrate phase and fill the cavities are N , m and NH , respectively.

The Langmuir constant can be calculated using Lennard-Jones and Devonshire cell theory (1939) or empirical correlation proposed by Parrish and Prausnitz (1972).

$$C_{jm} = \frac{A_{jm}}{T} \exp\left(\frac{B_{jm}}{T}\right) \tag{8}$$

This correlation is fitted for temperature range of 260–300 K.

Constants A and B of the current work are given in Table 1.

A proper EOS should be hired to obtain fugacity of component j in gas phase, Eq. (9). The applied EOS in the current study is introduced in “Equation of state” section.

$$f_j^v = \phi_j^v(P, T, y, \text{EOS}) \times P \times y_j \tag{9}$$

The chemical potential difference of water and virtual phase is:

$$\frac{\Delta\mu_w^{\beta-L}}{RT} = \frac{\Delta\mu_w^0}{RT_0} - \int_{T_0}^T \frac{\Delta h_w^{\beta-L}}{RT^2} dT + \int_{P_0}^P \frac{\Delta v_w^{\beta-L}}{RT} dP - \ln a_w \tag{10}$$

The molar enthalpy difference can be determined as:

$$\Delta h_w^{\beta-L} = \Delta h_w^{0,\beta-L} + \int_{T_0}^T \Delta C_p dT \tag{11}$$

Table 1 Coefficients of Langmuir constant

	$A \times e+3$ (K/atm)	B
Small cavity	0.7228	3187
Large cavity	23.35	2653

Table 2 Thermodynamic parameters of VdW-P

Properties	α'	ΔC_p^0 (cal/mol K)	$\Delta H_w^{0,\beta-L}$ (cal/mol)	$\Delta V_w^{0,\beta-L}$ (cm ³ /mol)
Value	- 0.0336	9.11	- 1161.3	4.6

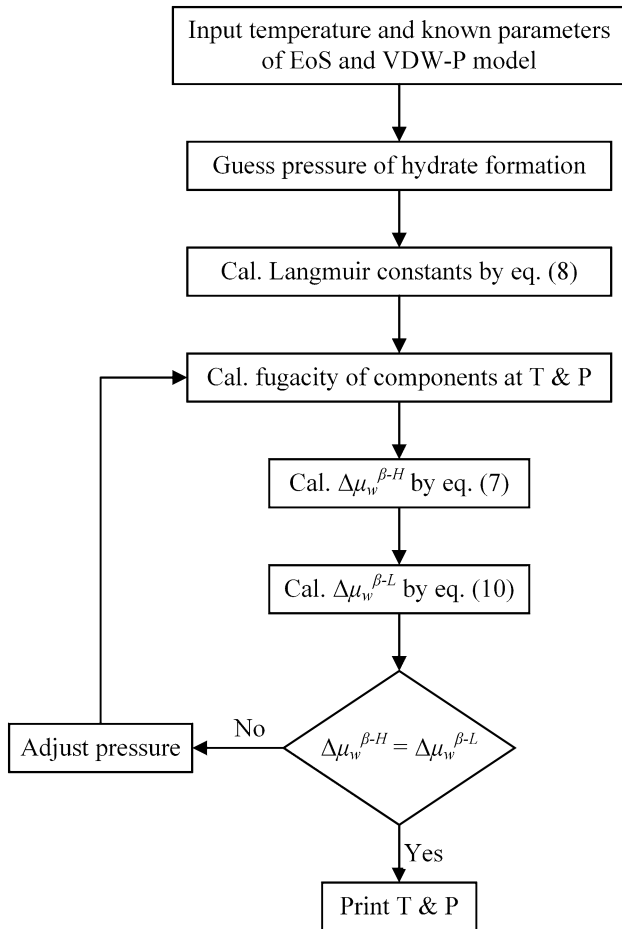


Fig. 1 Typical algorithm of VdW-P model

Also, heat capacity can be calculated as:

$$\Delta C_p = \Delta C_p^0 + \alpha' (T - T_0) \tag{12}$$

The required coefficients of above correlations are presented in Table 2 (Parrish and Prausnitz 1972).

The activity of water in liquid phase is presumed to be unit due to low solubility of methane in water. The calculation algorithm suggested by VdW-P model is shown in Fig. 1.

Equation of state

Six including cubic EOSs (van der Waals (VdW), Redlich–Kwong (RK), Soave–Redlich–Kwong (SRK) and Peng–Robinson (PR), Patel–Teja (PT) and Tsai–Jan (TJ))

Table 3 EOS and corresponding fugacity coefficients

EOSs	The cubic form and Virial EOS	References	Relations for fugacity coefficient	References
Virial	$Z = 1 + B/V + C/V^2$	Ghiasi (2012)	$\ln \phi = \frac{2B}{v} + \frac{1.5C}{v^2} - \ln Z$	Linga et al. (2009a)
VdW	$Z^3 - (1 + B)Z^2 + AZ - AB = 0$	Hammerschmidt (1934)	$\ln \phi = Z - 1 - \frac{a}{RTv} - \ln \left(Z \left(1 - \frac{b}{v} \right) \right)$	Linga et al. (2009a)
RK	$Z^3 - Z^2 + (A - B - B^2)Z - AB = 0$	Holder et al. (1988)	$\ln \phi = Z - 1 - \ln(Z - B) - \frac{A}{B} \ln \left(Z \left(1 - \frac{B}{Z} \right) \right)$	Linga et al. (2009a)
SRK	$Z^3 - Z^2 + (A - B - B^2)Z - AB = 0$	Kobayashi et al. (1987)	$\ln \phi = Z - 1 - \ln(Z - B) - \frac{A}{B} \ln \left(Z \left(1 - \frac{B}{Z} \right) \right)$	Linga et al. (2009a)
PR	$Z^3 - (1 + B)Z^2 + (A - 2B - 3B^2)Z - (AB - B^2 - B^3) = 0$	Koh et al. (2002)	$\ln \phi = Z - 1 - \ln(Z - B) - \frac{A}{2\sqrt{2}B} \ln \left(\frac{Z+2.414B}{Z-0.414B} \right)$	Linga et al. (2009a)
TJ	$Z^3 - (1 + B - 2C)Z^2 + (A - B^2 - 2BC - 2C)Z - (AB - B^2 - B^3) = 0$	Lennard-Jones and Devonshire (1939)	$\ln \phi = Z - 1 - \ln(Z - B) - \frac{A}{2qC} \ln \left(\frac{Z+(1+q)C}{Z+(1-q)C} \right)$, $q = (1 + (B/C)^2)^{0.5}$	Lennard-Jones and Devonshire (1939)
PT	$Z^3 + (C - 1)Z^2 + (A - B^2 - 2BC - B - C)Z - (AB - CB^2 - BC) = 0$	Konno et al. (2016)	$\ln \phi = Z - 1 - \ln(Z - B) + \frac{a}{2qN} \ln \left(\frac{Z+M}{Z+1+\frac{M}{2}} \right)^{+1/2}$ $M = \frac{b+c-N}{\frac{b+c}{RT} + N}$, $Q = \left(\frac{b+c}{2} + N \right) \frac{P}{RT}$, $B = bP/RT$	Konno et al. (2016)

along with Virial EOS are introduced in Table 3. The corresponding fugacity coefficients of each EOS are shown in Table 3. These EOSs were chosen because of their popularity in equilibrium thermodynamic modeling. The fugacity coefficients are needed for calculation of pressure and temperature of hydrate formation.

New correlation

In this work, genetic programming (GP) is manipulated to develop new mathematical correlation for methane hydrate formation temperature (Ganji et al. 2007). The origin of evolutionary algorithms is Darwinian Theory which is inspired by biological evolution (Mohamadi-Baghmolaei et al. 2016a). These algorithms grow according to survival of fittest. The mutation and crossover process, which are the random mechanisms, introduce the strongest genomes as parents of next generations (Linga et al. 2009a). In GP algorithm, the individuals are represented by trees. Indeed, this method is capable of reproducing a mathematical equation based on its tree structural mechanism, whereas other evolutionary algorithms are incapable or their flexibility is less pronounced (Zhong et al. 2016). A tree structural GP individual is displayed in Fig. 2. The prefixed notion of GP presented equation (Fig. 2) is shown by Eq. (13).

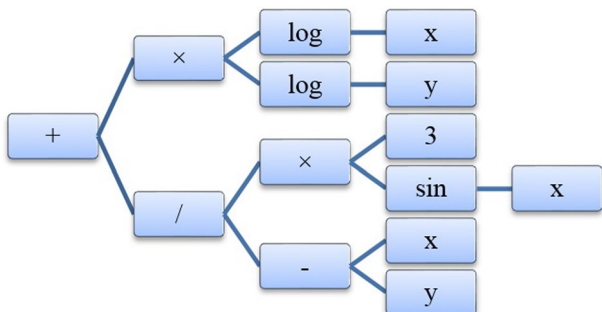
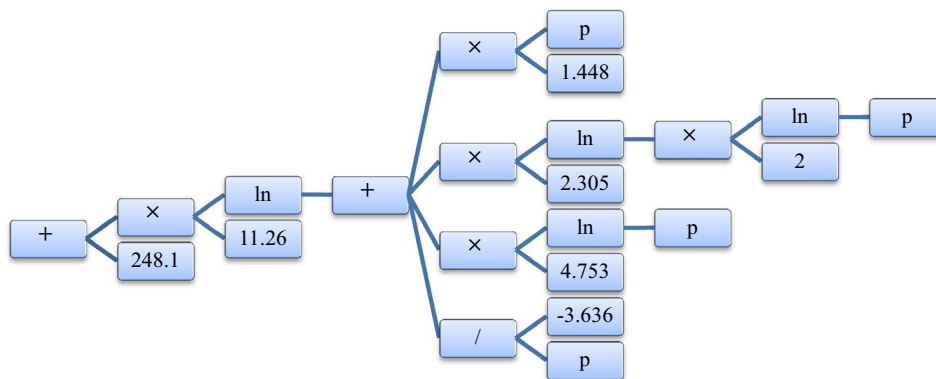


Fig. 2 Mutation process in GP

Fig. 3 Tree structure of new correlation



$$\text{Parent1} = \log(x) \cdot \log(y) + \frac{y-x}{3 \sin(x)} \tag{13}$$

The fundamental and detail concept of GP algorithm is described by Mohamadi-Baghmolaei et al. (2016b). Based on GP algorithm, a new correlation is developed to predict the hydrate formation temperature. The HFT (K) is correlated for pure methane as function of pressure (MPa). About 75% of experimental data are implemented for validation of correlation, and the remains and non-repetitive data are chosen to test the new correlation. Tree structure of new correlation is shown in Fig. 3.

Details of proposed correlation are as follows:

$$T = a + b \times \ln(A) \tag{14}$$

$$A = cp + d \times \ln(B) + e \times \ln(p) - f/p \tag{15}$$

$$B = g \times \ln(p) \tag{16}$$

The developed correlation covers a wide range existing input data ($259.1 \leq T(K) \leq 320.1$) and compensates other correlations which are mostly coverless range of input data. Despite the long and tedious conventional empirical correlations, the new developed correlation includes less involving terms. The proposed correlation is simple, which makes it profitable for academic and industrial proposes. Constants of new correlation (Eqs. 14–16) are given in Table 4.

Table 4 Constants of new correlation

Coeff.	Value
<i>a</i>	248.1
<i>b</i>	11.26
<i>c</i>	1.448
<i>d</i>	2.305
<i>e</i>	4.753
<i>f</i>	3.636
<i>g</i>	2

Table 5 Statistical information of data points

Property	Min.	Max.	Avg.	SD*
Temperature (K)	259.1	320.1	286.9	12.67
Pressure (MPa)	1.65	397	37.17	76.94

*Standard deviation

Results and discussion

In this study, VdW-P thermodynamic model (considering seven EOSs) and several empirical correlations are chosen to find the most accurate one. To do this, 101 experimental datasets for pure methane were extracted from open literature (Sloan and Koh 2007). The statistical characteristics of data are reported in Table 5. Different statistical errors functions are used to evaluate models and determine the most accurate one. These functions are defined in “Required parameters of EOS” appendix section.

Comparison of applying different EOSs in VdW-P model

Quantitative comparison of utilizing different EOSs in VdW-P model based on statistical errors is presented in Table 6 where the temperature range is 259.1–320.1 (K). It is observed that for the total temperature range, the SRK EOS has the least and preferable root-mean-squared error (RMSE) (41.1626). In contrast, PR has the maximum value RMSE (1.2987e+04) which may make it unsuitable for prediction of hydrate formation condition. It is worth mentioning that for the temperature range of 259.1–284.3 (K), the Virial EOS is the most precise EOS with respect to statistical errors reported in Table 5. On the other hand, at temperatures higher than 284.3–320.1 K the SRK EOS is suggested to be used in VdW-P (see Table 6).

The accuracy of EOS in VdW-P model can be recognized from Figs. 4 and 5 where predicted pressures and experimental data are displayed by different symbols.

The Langmuir constants were determined based on SRK EOS, which has best predictions for HFP of methane. The

Table 6 Statistical error of HFP using EOS

EOSs	$T \leq 284.3$			$284.3 \leq T$			$259.1 \leq T \leq 320.1$		
	R^2	RMSE	AARE	R^2	RMSE	AARE	R^2	RMSE	AARE
Virial	0.9880	0.0246	4.5495	0.5030	1.2209e+03	12.6382	0.6324	1.2209e+03	14.9818
RK	0.9810	0.0429	5.9936	0.9776	73.2635	8.9240	0.9789	73.2851	11.9505
VdW	0.9644	0.0896	7.7468	0.6235	417.5920	10.9393	0.6892	417.6372	14.8510
SRK	0.9852	0.0320	5.2796	0.9859	41.1465	6.4350	0.9887	41.1626	9.1010
PR	0.9771	0.0531	6.5240	0.5258	1.2987e+04	32.2215	0.5274	1.2987e+04	35.5159
TJ	0.9859	0.0302	5.1345	0.9123	458.9166	10.8965	0.9155	458.9318	13.4891
PT	0.9873	0.0266	4.7471	0.8632	911.7403	11.4415	0.8669	911.7537	13.8385

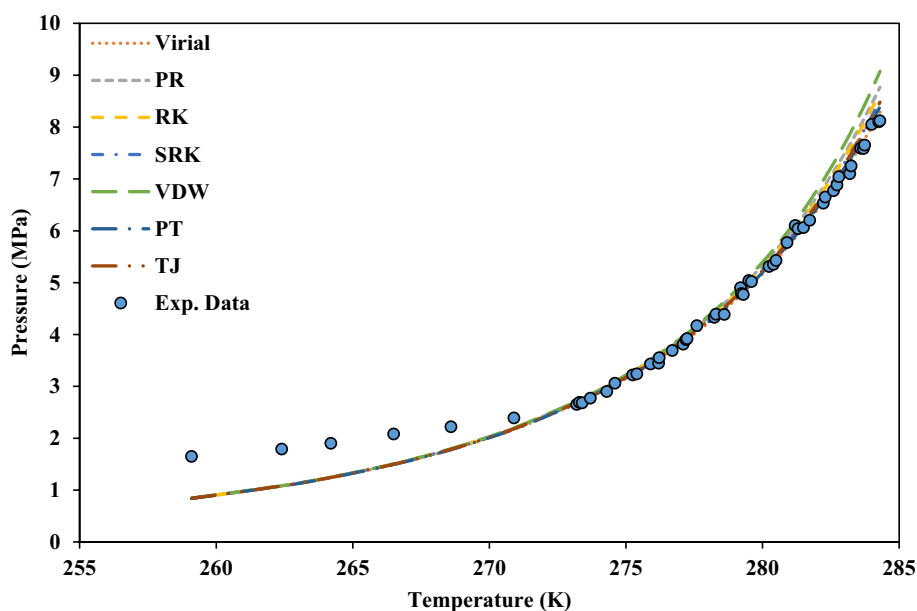
Fig. 4 Comparison between different EOSs used in VdW-P for $259.1 \leq T \leq 284.3$ K

Fig. 5 Comparison between different EOSs used in VdW-P for $284.3 \leq T \leq 320.1$ K

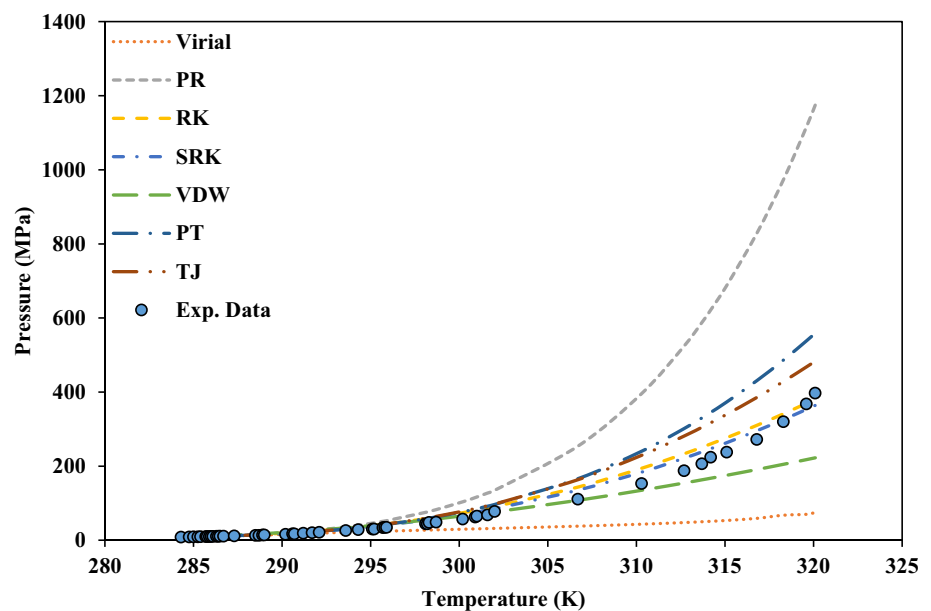


Table 7 Statistical errors of PR and Virial EOSs in comparison with SRK EOS

EOSs	RSS	AARE
PR	1.5420	0.3059
Virial	0.4477	0.2146

Table 8 Statistical error of HFP using empirical correlations for $259.1 \leq T \leq 320.1$

S	R^2	RMSE	AARE
HSCH	0.5683	129.9693	4.5487
Berge	0.9662	2.1431	0.3251
Holder et al.	0.4837	569.7024	16.4595
BV	0.2886	712.7525	11.8199
Ghayyem et al.	0.2989	431.9109	9.6792
Ghiasi	0.8478	6.7202	0.6999
TM	0.7354	19.6692	2.0549

accuracy lays behind the difference between calculated fugacities by each EOS. Calculated errors of fugacity by different EOSs are shown in Table 7.

As mentioned before, accuracy of calculated fugacities should be evaluated and compared by the fugacities determined from SRK EOS in which the experimental pressure and temperature are applied. The results shown in Table 7 confirm that calculated fugacity by PR and Virial EOSs at experimental temperature and pressure are not consistent with SRK EOS at temperature higher than 295 K; therefore, calculated HFP by these two EOSs has large statistical error.

Comparison between empirical correlations

Comparison between empirical correlations is given in Table 8. Of the seven correlations, the Berge has the least RMSE value (2.1431), followed by Ghiasi (Ghiasi 2012) with RMSE (6.7202). On the other side, Ghayyem et al. (2014) correlation shows a significant disagreement with experimental data. It should be mentioned that HSCH, BV, TM are the abbreviation form of Hammerschmidt (1934), Bahadori and Vuthaluru (2009), Towler and Mokhatab (2005) correlation, respectively. These correlations are introduced in “Empirical correlations” appendix section.

The accuracy of Berge correlation among others is clear in Fig. 6 where the high deviation of HSCH from experimental data is significantly apparent.

Evaluation of new correlation

The new developed correlation shows the highest agreement with experimental data, as shown in Table 9. The computed errors of developed correlation for validation and test steps are reported in Table 9.

Also, comparison between new correlation and experimental data is illustrated in Fig. 7. It is clear that the highest accuracy is observed in tracing experimental data using new correlation. As seen, total errors of proposed correlation compensate all reported empirical correlations and VdW-P models. The new correlation satisfied the experimental data well enough.

To compare best predicting method of HFP, scattered diagram of best empirical correlation, VdW-model and new correlation are depicted in Fig. 8. For temperature range of 259.1–284.3 K, the Virial EOS is the most accurate EOS.

Fig. 6 Comparison between empirical correlations

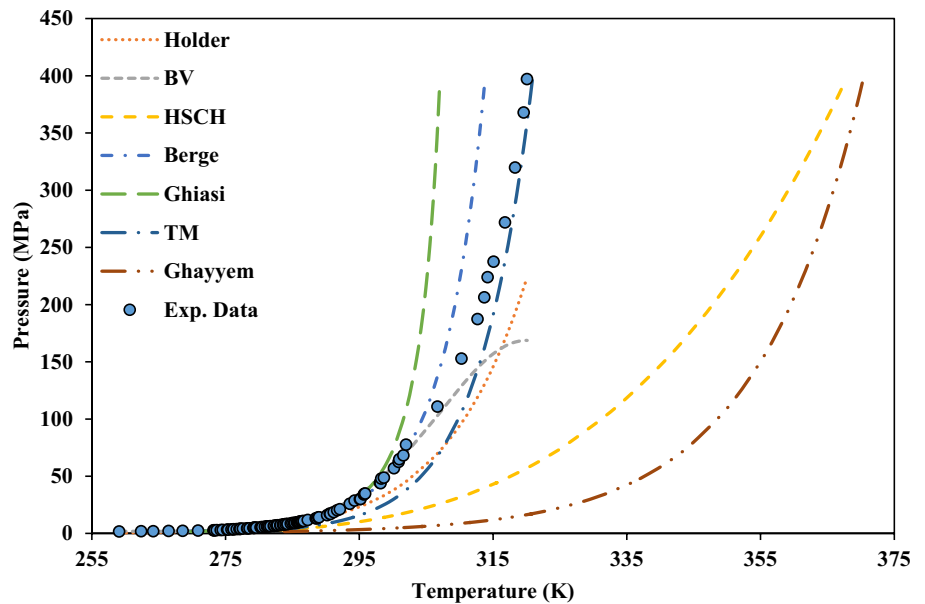


Table 9 Statistical error of HFP based on new correlation

New correlation	Train	Test	Overall
R^2	0.9991	0.9987	0.9990
RMSE	0.0733	0.0970	0.0794
AARE	0.1056	0.1118	0.1072

For overall temperature range (259.1–320.1 K), the SRK EOS has best results between other EOSs. In addition, Berge correlation is the most accurate one in comparison with other empirical correlations considering overall range of temperatures. Also, our new correlation is the best predictor between all other methods and equations.

Modified correlations

The modified HSCH correlation shows an improvement of predictability for HFP. It precedes all empirical correlation predictions. It is noteworthy that, the modified HSCH is more accurate than all models of VdW-P. Another modified correlation is that of Holder et al. although the modified Holder et al.’s correlation is better than the old version, but it is still less accurate in comparison with Berge and Ghiasi and TM correlations. The modified Holder et al.’s correlation convinces the experimental data much better than VdW-P models except for SRK EOS. The calculated errors for modified correlations are reported in Table 10. The modified correlations of HSCH and Holder et al. are:

$$T = 265.9744P^{0.0309} \tag{17}$$

Fig. 7 Comparison between new correlation and experimental data

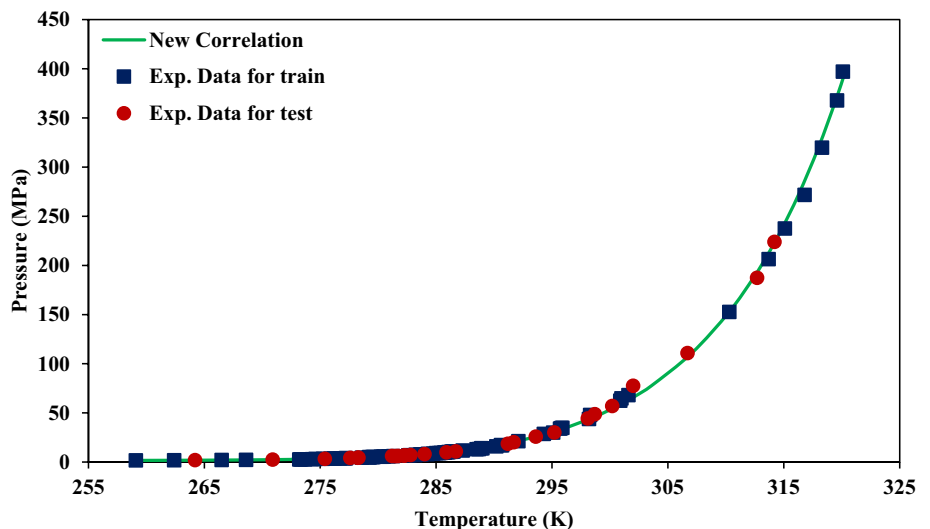


Fig. 8 Scattered diagrams of the best predicting methods

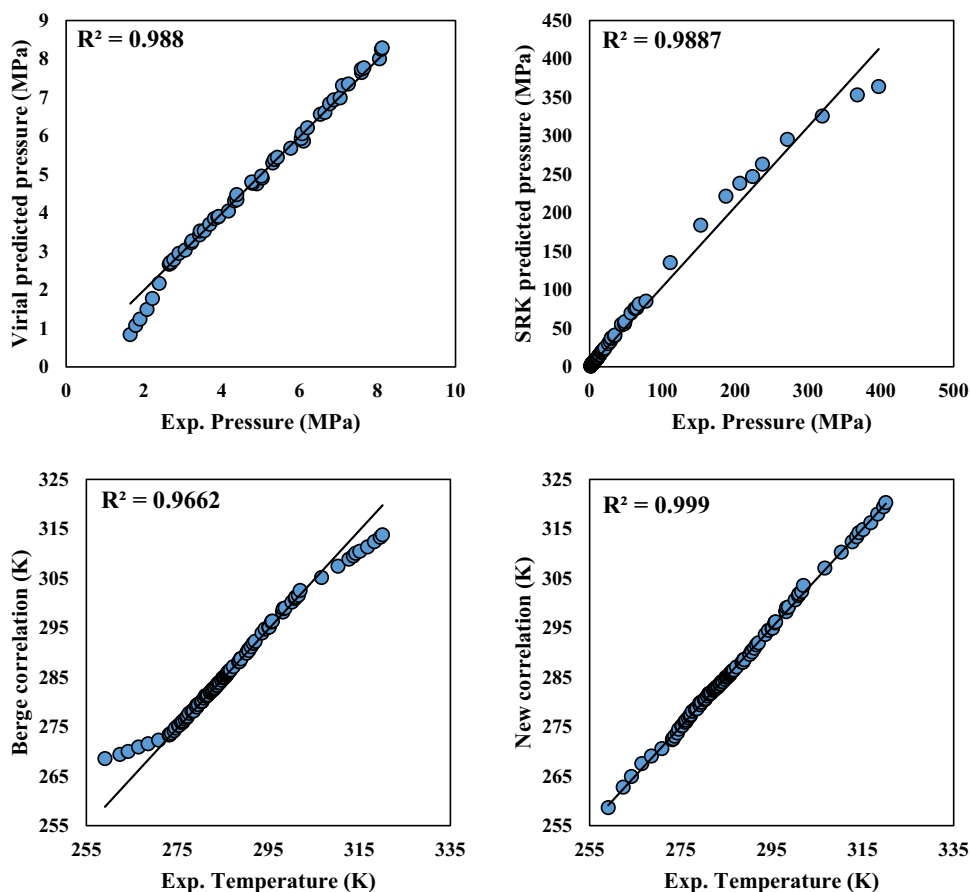


Table 10 Statistical error of HFP using modified empirical correlations

Empirical correlation	R^2	RMSE	AARE
Mod * HSCH	0.9777	1.6335	0.2998
Mod holder	0.9563	90.6184	10.0985

*Mod denotes modified

$$P = \exp \left(34.4077 + \frac{-9165.9451}{T} \right) \quad (18)$$

where temperature and pressure are reported in K and MPa.

Conclusion

In the current paper, the new simple correlation for prediction of hydrate formation temperature for temperature range of 259.1–320.1 (K) was developed. The computed statistical errors signify the excellence of proposed method in

comparison with common empirical correlations and application of different EOSs in VdW-P model. Also it has been noticed that for the range of $259.1 \leq T(K) \leq 284.3$ the Virial EOS is the best among other EOS, whereas for the temperature range of $284.3 \leq T(K) \leq 320.1$ the SRK EOS has the maximum consistency with experimental data. Of the seven empirical correlations, that of Berge is the most truthful. The simplicity and accuracy of proposed new correlation prepare the easiest way of methane HFT prediction among longsome VdW-P methods and complicated correlations.

Open Access This article is distributed under the terms of the Creative Commons Attribution 4.0 International License (<http://creativecommons.org/licenses/by/4.0/>), which permits unrestricted use, distribution, and reproduction in any medium, provided you give appropriate credit to the original author(s) and the source, provide a link to the Creative Commons license, and indicate if changes were made.

Appendix 1: Empirical correlations

Berge proposed another correlation by including the gas specific gravity (Berge 1986). This correlation is written in the form of Eqs. (19) and (20) for two ranges of specific gravity. For $0.555 \leq \gamma \leq 0.58$

$$T = \left(-96.03 + 25.37 \ln(P) - 0.64 \ln(P)^2 + \frac{(\gamma - 0.555)}{0.025} \right) \times \left(80.61P + \frac{1.16 \times 10^4}{P + 599.16} - 96.03 + 25.37 \ln(P) - 0.64 \ln(P)^2 \right) \quad (19)$$

For $0.58 \leq \gamma \leq 1$

$$T = \frac{-1.23 \times 10^4 + 80.61P - 2.1 \times 10^4 - \frac{1.22 \times 10^3}{\gamma - 0.535} - \frac{1.71 \times 10^3}{\gamma - 0.509}}{\left(P - 260.42 - \frac{15.18}{\gamma - 0.535} \right)} \quad (20)$$

where the temperature and pressure are in °F and psi, respectively. Motiee offered a correlation as function of pressure (kPa) and gas gravity for prediction of HFT (°C) (1991).

$$T = -283.24469 + 78.99667 \log P - 5.352544(\log P)^2 + 349.473877 \times \gamma - 150.854675 \times \gamma^2 - 27.604065 \times \gamma \log(P) \quad (21)$$

Another correlation for prediction of HFT was introduced by Towler and Mokhatab (TM) (2005).

$$T = 13.47 \ln P + 34.27 \ln \gamma - 1.675 \ln P \times \ln \gamma - 20.35 \quad (22)$$

Bahadori and Vuthaluru (BV) presented specific equations for prediction of temperature and pressure of hydrate formation as function of molecular weight (2009).

$$T = \exp\left(a + \frac{b}{P} + \frac{c}{P^2} + \frac{d}{P^3}\right) \quad (23)$$

$$P = \exp\left(a + \frac{b}{T} + \frac{c}{T^2} + \frac{d}{T^3}\right) \quad (24)$$

where P and T are in kPa and K. The required parameters of Eqs. (23) and (24) are listed below:

$$a = A_1 + B_1 M_w + C_1 M_w^2 + D_1 M_w^3 \quad (25)$$

$$b = A_2 + B_2 M_w + C_2 M_w^2 + D_2 M_w^3 \quad (26)$$

$$c = A_3 + B_3 M_w + C_3 M_w^2 + D_3 M_w^3 \quad (27)$$

$$d = A_4 + B_4 M_w + C_4 M_w^2 + D_4 M_w^3 \quad (28)$$

The above coefficients are reported by Bahadori and Vuthaluru.

Gheyyem et al. introduced an empirical correlation based on regression method. Their correlation was function of pressure (psi) and gas gravity to give HFT in °F.

$$T = a + \frac{b}{\gamma} + c \ln P + d \exp(\gamma^8) + e \ln(P)^2 + f \ln(P) \times \exp(\gamma^h) \quad (29)$$

The coefficients of Ghayyem correlation have been reported in his paper (Ghayyem et al. 2014).

Appendix 2: Required parameters of EOS

The needed parameters for cubic EOS form are presented in Tables 11, 12 and 13.

Where α , for SRK and PR EOS, are presented by Eqs. (30) and (31), respectively:

$$\alpha = \left(1 + (0.48508 + 1.55171\omega - 0.15613\omega^2) \left(1 - \frac{T}{T_c} \right)^{0.5} \right)^2 \quad (30)$$

$$\alpha = \left(1 + (0.37464 + 1.54226\omega - 0.26992\omega^2) \left(1 - \frac{T}{T_c} \right)^{0.5} \right)^2 \quad (31)$$

$$\Omega_b^3 + (1 - 3\zeta_c)\Omega_b^2 + (1 - 3\zeta_c + 3\zeta_c^2)\Omega_b - \zeta_c^3 = 0 \quad (32)$$

$$\Omega_a = \Omega_b^2 + \Omega_b + \zeta_c^3 / \Omega_b \quad (33)$$

$$\Omega_c = (\Omega_b - 3\zeta_c + 1) / 2 \quad (34)$$

$$\zeta_c = 0.32011 - 0.04539\omega + 0.01631\omega^2 \quad (35)$$

$$\alpha = (1 + m(1 - T_r^{0.5}))^2 \quad (36)$$

$$m = m_0 + (4T_r - m_0 - 2)^2 / 50 \quad \text{for } T_r \leq 1 \quad (37)$$

$$m = m_0 + (2 - m_0)^2 / 50 \quad \text{for } T_r > 1 \quad (38)$$

$$m_0 = 0.375 + 1.546\omega - 0.292\omega^2 \quad (39)$$

Table 11 VdW, RK, SRK, and PR EOS parameters

EOSs	A	B	a	b	References
VdW	$\frac{aP}{R^2 T^2}$	$\frac{bP}{RT}$	$0.421875 \frac{R^2 T_c^2}{P_c}$	$0.125 \frac{RT_c}{P_c}$	Linga et al. (2009a)
RK	$\frac{ap}{R^2 T^{2.5}}$	$\frac{bp}{RT}$	$0.42747 \frac{R^2 T_c^{2.5}}{P_c}$	$0.08664 \frac{RT_c}{P_c}$	Linga et al. (2009a)
SRK	$\frac{aap}{R^2 T^2}$	$\frac{bp}{RT}$	$0.42747 \frac{R^2 T_c^{2.5}}{P_c}$	$0.08664 \frac{RT_c}{P_c}$	Linga et al. (2009a)
PR	$\frac{aap}{R^2 T^2}$	$\frac{bp}{RT}$	$0.457235 \frac{R^2 T_c^2}{P_c}$	$0.077796 \frac{RT_c}{P_c}$	Linga et al. (2009a)

Table 12 TJ EOS parameters

EOS	A	B	C	a (T)	a _c	b	c	Reference
TJ	$\frac{a(T)P}{R^2T^2}$	$\frac{bP}{RT}$	$\frac{cP}{RT}$	$a_c \cdot \alpha(T)$	$\Omega_a(R^2T_c^2/P_c)$	$\Omega_b(RT_c/P_c)$	$\Omega_c(RT_c/P_c)$	Lennard-Jones and Devonshire (1939)

Table 13 PT EOS parameters

EOS	A	B	C	a (T)	a _c	b	c	Reference
PT	$\frac{a(T)P}{R^2T^2}$	$\frac{bP}{RT}$	$\frac{cP}{RT}$	$a_c \cdot \alpha(T)$	$\Omega_a(R^2T_c^2/P_c)$	$\Omega_b(RT_c/P_c)$	$\Omega_c(RT_c/P_c)$	Konno et al. (2016)

$$\Omega_b^3 + (2 - 3\zeta_c)\Omega_b^2 + 3\zeta_c^2\Omega_b - \zeta_c^3 = 0 \tag{40}$$

$$\Omega_a = 3\zeta_c^2 + 3(1 - 2\zeta_c)\Omega_b + \Omega_b^2 + 1 - 3\zeta_c \tag{41}$$

$$\Omega_c = 1 - \zeta_c \tag{42}$$

$$\zeta_c = 0.329032 - 0.076799\omega + 0.0211947\omega^2 \tag{43}$$

$$\alpha = (1 + F(1 - T_r^{0.5}))^2 \tag{44}$$

$$F = 0.452413 + 1.30982\omega - 0.295937\omega^2 \tag{45}$$

Appendix 3: Types of errors

Coefficient of determination

$$R^2 = 1 - \frac{\sum_{i=1}^N (Z_i^{\text{Pred}} - Z_i^{\text{exp}})^2}{\sum_{i=1}^N (Z_i^{\text{Pred}} - \text{average}(Z_i^{\text{exp}}))^2} \tag{46}$$

Average absolute relative error

$$\text{AARE}\% = \frac{100}{N} \sum_{i=1}^N \left(\left| \frac{Z_i^{\text{Pred}} - Z_i^{\text{exp}}}{Z_i^{\text{exp}}} \right| \right) \tag{47}$$

Root-mean-square error

$$\text{RMSE} = \left(\frac{\sum_{i=1}^N (Z_i^{\text{Pred}} - Z_i^{\text{exp}})^2}{N} \right)^{\frac{1}{2}} \tag{48}$$

Residual sum of square

$$\text{RSS} = \sum_{i=1}^N (Z_i^{\text{Pred}} - Z_i^{\text{exp}})^2 \tag{49}$$

References

Amin JS, Nikkiah S, Veiskarami M (2015) A statistical method for assessment of the existing correlations of hydrate forming conditions. *J Energy Chem* 24:93–100

Babu P, Kumar R, Linga P (2013) Pre-combustion capture of carbon dioxide in a fixed bed reactor using the clathrate hydrate process. *Energy* 50:364–373

Bahadori A, Vuthaluru HB (2009) A novel correlation for estimation of hydrate forming condition of natural gases. *J Nat Gas Chem* 18:453–457

Berge B (1986) Hydrate predictions on a microcomputer. Petroleum industry application of microcomputers. Society of Petroleum Engineers, Silvercreek, Colorado. <https://doi.org/10.2118/15306-MS>

Carroll J (2014) Natural gas hydrates: a guide for engineers. Gulf Professional Publishing, Houston

Chari VD, Sharma DV, Prasad PS, Murthy SR (2013) Methane hydrates formation and dissociation in nano silica suspension. *J Nat Gas Sci Eng* 11:7–11

Chen G-J, Guo T-M (1996) Thermodynamic modeling of hydrate formation based on new concepts. *Fluid Phase Equilib* 122:43–65

Collett TS (2002) Energy resource potential of natural gas hydrates. *AAPG Bull* 86:1971–1992

Collett TS, Boswell R, Cochran JR, Kumar P, Lall M, Mazumdar A, Ramana MV, Ramprasad T, Riedel M, Sain K (2014) Geologic implications of gas hydrates in the offshore of India: results of the national gas hydrate program expedition 01. *Mar Pet Geol* 58:3–28

Elgibaly AA, Elkamel AM (1998) A new correlation for predicting hydrate formation conditions for various gas mixtures and inhibitors. *Fluid Phase Equilib* 152:23–42

Fujii T, Suzuki K, Takayama T, Tamaki M, Komatsu Y, Konno Y, Yoneda J, Yamamoto K, Nagao J (2015) Geological setting and characterization of a methane hydrate reservoir distributed at the first offshore production test site on the Daini-Atsumi Knoll in the eastern Nankai Trough, Japan. *Mar Pet Geol* 66:310–322

Ganji H, Manteghian M, Omidkhah M, Mofrad HR (2007) Effect of different surfactants on methane hydrate formation rate, stability and storage capacity. *Fuel* 86:434–441

Garapati N, Anderson BJ (2014) Statistical thermodynamics model and empirical correlations for predicting mixed hydrate phase equilibria. *Fluid Phase Equilib* 373:20–28

Ghayyem M, Izadmehr M, Tavakoli R (2014) Developing a simple and accurate correlation for initial estimation of hydrate formation temperature of sweet natural gases using an eclectic approach. *J Nat Gas Sci Eng* 21:184–192

Ghiasi MM (2012) Initial estimation of hydrate formation temperature of sweet natural gases based on new empirical correlation. *J Nat Gas Chem* 21:508–512

- Hammerschmidt E (1934) Formation of gas hydrates in natural gas transmission lines. *Ind Eng Chem* 26:851–855
- Holder G, Zetts S, Pradhan N (1988) Phase behavior in systems containing clathrate hydrates: a review. *Rev Chem Eng* 5:1–70
- Kobayashi R, Song KY, Sloan ED (1987) Phase behavior of water/hydrocarbon systems. *Pet Eng Handb* 25:e13
- Koh C, Westacott R, Zhang W, Hirachand K, Creek J, Soper A (2002) Mechanisms of gas hydrate formation and inhibition. *Fluid Phase Equilib* 194:143–151
- Konno Y, Masuda Y, Akamine K, Naiki M, Nagao J (2016) Sustainable gas production from methane hydrate reservoirs by the cyclic depressurization method. *Energy Convers Manag* 108:439–445
- Lennard-Jones J, Devonshire A (1939) Critical and co-operative phenomena. IV. A theory of disorder in solids and liquids and the process of melting. In: *Proceedings of the Royal Society of London. Series A, mathematical and physical sciences*, pp 464–484
- Liang M, Chen G, Sun C, Yan L, Liu J, Ma Q (2005) Experimental and modeling study on decomposition kinetics of methane hydrates in different media. *J Phys Chem B* 109:19034–19041
- Lim SH, Riffat SB, Park SS, Oh SJ, Chun W, Kim NJ (2014) Enhancement of methane hydrate formation using a mixture of tetrahydrofuran and oxidized multi-wall carbon nanotubes. *Int J Energy Res* 38:374–379
- Linga P, Haligva C, Nam SC, Ripmeester JA, Englezos P (2009a) Gas hydrate formation in a variable volume bed of silica sand particles. *Energy Fuels* 23:5496–5507
- Linga P, Haligva C, Nam SC, Ripmeester JA, Englezos P (2009b) Recovery of methane from hydrate formed in a variable volume bed of silica sand particles. *Energy Fuels* 23:5508–5516
- Mohamadi-Baghmolaei M, Mahmoudy M, Jafari D, Mohamadi-Baghmolaei R, Tabkhi F (2014) Assessing and optimization of pipeline system performance using intelligent systems. *J Nat Gas Sci Eng* 18:64–76
- Mohamadi-Baghmolaei M, Azin R, Osfuri S, Mohamadi-Baghmolaei R, Zarei Z (2015) Prediction of gas compressibility factor using intelligent models. *Nat Gas Ind B* 2:283–294
- Mohamadi-Baghmolaei M, Azin R, Sakhaei Z, Mohamadi-Baghmolaei R, Osfouri S (2016a) Novel method for estimation of gas/oil relative permeabilities. *J Mol Liq* 223:1185–1191
- Mohamadi-Baghmolaei M, Azin R, Zarei Z, Osfouri S (2016b) Presenting decision tree for best mixing rules and Z-factor correlations and introducing novel correlation for binary mixtures. *Petroleum* 2:289–295
- Motiee M (1991) Estimate possibility of hydrates. *Hydrocarb Process* 70:98–99
- Park SS, Kim NJ (2010) Multi-walled carbon nano tubes effects for methane hydrate formation. In: 2010 the 2nd international conference on computer and automation engineering (ICCAE), IEEE
- Parrish WR, Prausnitz JM (1972) Dissociation pressures of gas hydrates formed by gas mixtures. *Ind Eng Chem Process Des Dev* 11:26–35
- Pasieka J, Coulombe S, Servio P (2013) Investigating the effects of hydrophobic and hydrophilic multi-wall carbon nanotubes on methane hydrate growth kinetics. *Chem Eng Sci* 104:998–1002
- Patel NC, Teja AS (1982) A new cubic equation of state for fluids and fluid mixtures. *Chem Eng Sci* 37:463–473
- Peng D-Y, Robinson DB (1976) A new two-constant equation of state. *Ind Eng Chem Fundam* 15:59–64
- Prausnitz JM, Lichtenthaler RN, deAzevedo EG (1998) *Molecular thermodynamics of fluid-phase equilibria*. Pearson Education, London
- Redlich O, Kwong JN (1949) On the thermodynamics of solutions. V. An equation of state. Fugacities of gaseous solutions. *Chemical reviews* 44:233–244
- Ruppel C, Boswell R, Jones E (2008) Scientific results from Gulf of Mexico gas hydrates Joint Industry Project Leg 1 drilling: introduction and overview. *Mar Pet Geol* 25:819–829
- Ryu B-J, Collett TS, Riedel M, Kim GY, Chun J-H, Bahk J-J, Lee JY, Kim J-H, Yoo D-G (2013) Scientific results of the second gas hydrate drilling expedition in the Ulleung basin (UBGH2). *Mar Pet Geol* 47:1–20
- Siangsai A, Rangsunvigit P, Kitiyanan B, Kulprathipanja S (2014) Improved methane hydrate formation rate using treated activated carbon and tetrahydrofuran. *J Chem Eng Jpn* 47:352–357
- Siangsai A, Rangsunvigit P, Kitiyanan B, Kulprathipanja S, Linga P (2015) Investigation on the roles of activated carbon particle sizes on methane hydrate formation and dissociation. *Chem Eng Sci* 126:383–389
- Sloan ED Jr, Koh C (2007) *Clathrate hydrates of natural gases*. CRC Press, Boca Raton
- Soave G (1972) Equilibrium constants from a modified Redlich-Kwong equation of state. *Chem Eng Sci* 27:1197–1203
- Towler B, Mokhatab S (2005) Quickly estimate hydrate formation conditions in natural gases. *Hydrocarb Process* 84:61–62
- Tsai FN, Jan DS (1990) A three-parameter cubic equation of state for fluids and fluid mixtures. *Can J Chem Eng* 68:479–486
- Van der Waals JD (1873) *Over de continuïteit van den gas-en vloeistof-toestand*. AW Sijthoff, Leiden
- Van der Waals J, Platteeuw J (2007) Clathrate solutions. *Adv Chem Phys* 2:1–57
- Vedachalam N, Srinivasalu S, Rajendran G, Ramadass G, Atmanand M (2015) Review of unconventional hydrocarbon resources in major energy consuming countries and efforts in realizing natural gas hydrates as a future source of energy. *J Nat Gas Sci Eng* 26:163–175
- Wilcox WI, Carson D, Katz D (1941) Natural gas hydrates. *Ind Eng Chem* 33:662–665
- Yan L, Chen G, Pang W, Liu J (2005) Experimental and modeling study on hydrate formation in wet activated carbon. *J Phys Chem B* 109:6025–6030
- Zhong D-L, Li Z, Lu Y-Y, Wang J-L, Yan J (2015) Evaluation of CO₂ removal from a CO₂ + CH₄ gas mixture using gas hydrate formation in liquid water and THF solutions. *Appl Energy* 158:133–141
- Zhong D-L, Ding K, Lu Y-Y, Yan J, Zhao W-L (2016) Methane recovery from coal mine gas using hydrate formation in water-in-oil emulsions. *Appl Energy* 162:1619–1626

Publisher's Note Springer Nature remains neutral with regard to jurisdictional claims in published maps and institutional affiliations.